Planar Hall effect bridge sensors with NiFe/Cu/IrMn stack optimized for self-field magnetic bead detection

Henriksen, Anders Dahl; Rizzi, Giovanni; Hansen, Mikkel Fougt

Published in:
Journal of Applied Physics

Link to article, DOI:
10.1063/1.4943033

Publication date:
2016

Document Version
Publisher's PDF, also known as Version of record

AIP | Journal of Applied Physics

Planar Hall effect bridge sensors with NiFe/Cu/IrMn stack optimized for self-field magnetic bead detection

Anders Dahl Henriksen, Giovanni Rizzi, and Mikkel Fougt Hansen

Citation: Journal of Applied Physics **119**, 093910 (2016); doi: 10.1063/1.4943033
View online: http://dx.doi.org/10.1063/1.4943033
View Table of Contents: http://scitation.aip.org/content/aip/journal/jap/119/9?ver=pdfcov
Published by the AIP Publishing

Planar Hall effect bridge sensors with NiFe/Cu/IrMn stack optimized for self-field magnetic bead detection

Anders Dahl Henriksen, Giovanni Rizzi, and Mikkel Fougt Hansen[a)]
Department of Micro- and Nanotechnology, Technical University of Denmark, DTU Nanotech, Building 345 East, DK-2800 Kongens, Lyngby, Denmark

(Received 5 October 2015; accepted 17 February 2016; published online 4 March 2016)

The stack composition in trilayer Planar Hall effect bridge sensors is investigated experimentally to identify the optimal stack for magnetic bead detection using the sensor self-field. The sensors were fabricated using exchange-biased stacks $Ni_{80}Fe_{20}(t_{FM})/Cu(t_{Cu})/Mn_{80}Ir_{20}(10\,nm)$ with $t_{FM} = 10$, 20, and 30 nm, and $0 \le t_{Cu} \le 0.6$ nm. The sensors were characterized by magnetic hysteresis measurements, by measurements of the sensor response vs. applied field, and by measurements of the sensor response to a suspension of magnetic beads magnetized by the sensor self-field due to the sensor bias current. The exchange bias field was found to decay exponentially with t_{Cu} and inversely with t_{FM}. The reduced exchange field for larger values of t_{FM} and t_{Cu} resulted in higher sensitivities to both magnetic fields and magnetic beads. We argue that the maximum magnetic bead signal is limited by Joule heating of the sensors and, thus, that the magnetic stacks should be compared at constant power consumption. For a fixed sensor geometry, the figure of merit for this comparison is the magnetic field sensitivity normalized by the sensor bias voltage. In this regard, we found that sensors with $t_{FM} = 20$ nm or 30 nm outperformed those with $t_{FM} = 10$ nm by a factor of approximately two, because the latter have a reduced AMR ratio. Further, the optimum layer thicknesses, $t_{Cu} \approx 0.6$ nm and $t_{FM} = 20$–30 nm, gave a 90% higher signal compared to the corresponding sensors with $t_{Cu} = 0$ nm. © *2016 AIP Publishing LLC*.
[http://dx.doi.org/10.1063/1.4943033]

I. INTRODUCTION

Magnetoresistive biosensors are promoted as an attractive approach to perform molecular diagnostics.[1,2] In these, magnetic beads are usually used as specific labels that bind to the target analyte, and because the biological sample provides no magnetic background signal, the analyte may be detected in real-time with high sensitivity and specificity.[3–8]

Magnetoresistive biosensors based on the planar Hall effect,[9–11] magnetic tunneling effect,[12,13] or giant magnetoresistance effect[4–6] have been proposed for this application. We have previously demonstrated the use of planar Hall effect bridge (PHEB) magnetic field sensors in both volume- and surface-based detection schemes,[7,14,15] and how the sensor design can be optimized towards such diverse applications.[16] In these studies, the magnetic beads were magnetized by the sensor self-field arising from the bias current passed through the sensor. This approach has two clear advantages: (1) No external magnetic field generators are needed. This simplifies the setup and also enables operation at frequencies up to the MHz range.[17] (2) As opposed to magnetic beads magnetized by a homogeneous external magnetic field, the signal from a magnetic bead has the same sign irrespective of the position of the magnetic bead relative to the sensor, and therefore, signal cancelation effects are avoided.[19,20] The magnetic bead signal obtained using the self-field detection approach is proportional to the square of the sensor bias current,[19] and therefore, it is desirable to use a high bias current.

Introduction of a noble metal spacer layer between the ferromagnet and the antiferromagnet in an exchange-biased permalloy stack has been shown to weaken the coupling between magnetic layers.[21] This has been used to construct trilayer planar Hall effect (PHE) sensors, where a 0.2 nm thick Cu spacer layer was observed to increase the sensitivity 7 times.[23] Hung *et al.*[24] studied trilayer PHE sensors with a Cu spacer and showed a reduced exchange bias for increasing copper thickness but also an increased current shunting. They concluded that a 0.12 nm thick copper layer was optimal for magnetic field sensing. A similar trilayer stack was later used in multi-ring planar Hall effect bridge sensors.[25]

The maximum signal that can be obtained from a sensor constructed from a given stack depends not only on the low-field sensitivity of the sensor but also on the maximum applicable sensor bias current. Thus, it is not *a priori* clear whether the optimum magnetic stack for magnetic field detection is also the best stack for detection of magnetic beads using the sensor self-field. Therefore, there is a need for a figure of merit that can be used to compare different sensor stacks for this detection scheme.

Here, we first investigate the effect of the sensor stack composition in trilayer planar Hall effect bridge sensors of a fixed geometry on the magnetic field sensitivity. Compared to previous work in the literature,[23,24] we expand the study to include a variation of both the permalloy and copper layer thicknesses. The sensor stacks are characterized using vibrating sample magnetometry (VSM) and analysis of the sensor

[a)]Electronic mail: Mikkel.Hansen@nanotech.dtu.dk

response vs. magnetic field in terms of a single domain model. We discuss the use of the sensors for magnetic field detection under different electrical operation conditions. Further, we measure the signal from the sensors from magnetic beads magnetized by the sensor self-field and discuss the influence of the stack composition on the maximum bead signal obtainable using a self-field detection scheme.

II. THEORY

A. Sensor design and response vs. magnetic field

In this work, we characterize PHEB sensors with four magnetoresistive elements in a Wheatstone bridge configuration (Fig. 1(a)).[26] Figure 1(b) shows the cross-section of each resistor. The magnetic stack is based on a ferromagnetic layer of permalloy ($Ni_{80}Fe_{20}$) that exhibits anisotropic magnetoresistance (AMR). The ferromagnetic layer is exchange-pinned along the x-direction using an antiferromagnetic $Mn_{80}Ir_{20}$ layer. A layer of copper is introduced between the ferromagnetic and antiferromagnetic layers to weaken the exchange bias. The resistivity of the sensor elements is dominated by the ferromagnetic layer. The resistivities of the stack when the magnetization and current are parallel and perpendicular, respectively, are denoted as $\rho_{\parallel}$ and $\rho_{\perp}$. Assuming a single magnetic domain state in each element with an in-plane angle of magnetization θ to the x-axis, the resistances of the elements $R_{\pm}$ in Fig. 1(a) are[7]

$$R_{\pm}(\theta) = \frac{l}{wt}\rho_{\text{avg}}\left(1 \pm \frac{\Delta\rho}{\rho_{\text{avg}}}\frac{\sin(2\theta)}{2}\right). \tag{1}$$

Here, l, w, and t, are the resistor length, width, and thickness; $\rho_{\text{avg}} = (\rho_{\parallel} + \rho_{\perp})/2$ is the average resistivity of the stack and $\Delta\rho = \rho_{\parallel} - \rho_{\perp}$.

When biased by a constant current I_x, the voltage across the PHEB sensor bridge depends on the magnetization angle θ.[26] However, due to shape anisotropy, the bridge elements with positive and negative slopes in Fig. 1 may have different angles of magnetization, θ_+ and θ_-, respectively. In this case, the bridge output is

$$V_y = I_x R_{\text{b}} \frac{\Delta\rho}{\rho_{\text{avg}}}\left[\sin(2\theta_+) + \sin(2\theta_-)\right]/4 \tag{2}$$

with $R_{\text{b}} = \frac{l}{wt}\rho_{\text{avg}}$. For negligible shape anisotropy $\theta_+ = \theta_- = \theta$ and small values of θ, the bridge output is proportional to θ.[27] It should be noted that the resistances of the individual elements depend on the magnetic field, whereas $R_+(\theta) + R_-(\theta) = 2R_{\text{b}}$ is independent of the magnetic field as long as the two elements have the same magnetization orientation. Thus, the bridge resistance R_{b} is constant. This ensures that sensors biased by a constant voltage also have a constant current irrespective of the magnetic field, i.e., $V_x = R_{\text{b}} I_x$.

The angle of magnetization, θ, is obtained by minimizing the magnetic energy density, u. In a homogeneous external magnetic field, B_y, along the y-axis, the normalized energy density is[27]

$$\tilde{u}_{\pm} = \frac{u_{\pm}}{M_s} = -B_y \sin\theta_{\pm} - B_{\text{ex}}\cos\theta_{\pm} - \frac{1}{2}B_{\text{K}}\cos^2\theta_{\pm} - \frac{1}{2}B_{\text{sh}}\cos^2\left(\pm\frac{\pi}{4} - \theta_{\pm}\right). \tag{3}$$

Here, M_s is the saturation magnetization, B_{ex} is the exchange bias field, B_{K} is the anisotropy field, and B_{sh} is the shape anisotropy field. For negligible shape anisotropy and low applied magnetic fields, Eq. (3) is minimized for

$$\theta \approx \frac{B_y}{B_{\text{ex}} + B_{\text{K}}}, \tag{4}$$

when B_{sh} dominates, the values of $\theta_{\pm}$ will approach $\pm\pi/4$. When $B_{\text{sh}} < (B_{\text{ex}} + B_{\text{K}})$, the sensor response is anhysteretic, and we can define a unique normalized low-field sensitivity as

$$\tilde{S}_0 = \frac{1}{I_x R_{\text{b}}}\frac{\partial V_y}{\partial B_y}\Big|_{B_y=0}. \tag{5}$$

$\tilde{S}_0$ [T^{-1}] combines the influence of the AMR ratio, the shape anisotropy, and the exchange bias on the low-field sensitivity. The low-field signals from current-biased and voltage-biased sensors, respectively, become

$$V_y = (I_x R_{\text{b}})\tilde{S}_0 B_y = V_x \tilde{S}_0 B_y. \tag{6}$$

For negligible shape anisotropy, insertion of Eqs. (2) and (4) in Eq. (6) yields

$$\tilde{S}_0 = \frac{\Delta\rho}{\rho_{\text{avg}}}\frac{1}{B_{\text{ex}} + B_{\text{K}}}. \tag{7}$$

As the exchange field is an interface effect, B_{ex} is expected to be inversely proportional to t_{FM}.[28] Gökemeijer *et al.*[21]

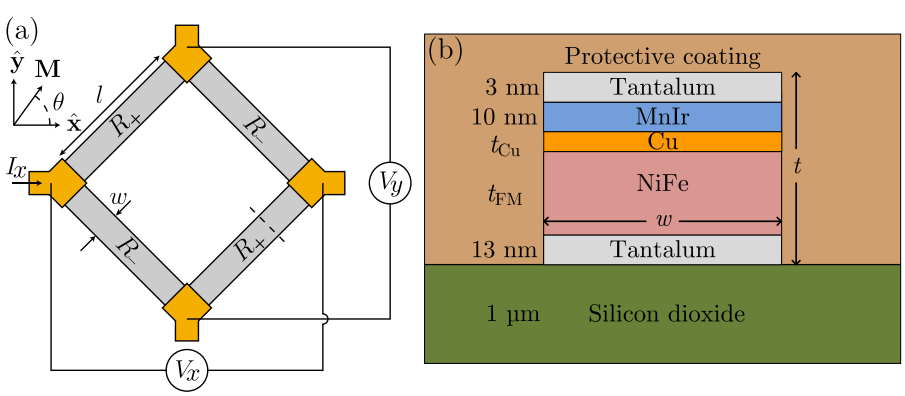

FIG. 1. (a) Illustration of the PHEB sensors with definitions of parameters and coordinate system. The grey and yellow colors indicate the sensor and contact stacks, respectively. (b) Illustration of the magnetic stack cross-section at the dashed line in (a).

have systematically studied the effect of a non-magnetic conducting spacer on the exchange bias field and found that the exchange bias field decreased exponentially with the thickness of the spacer. Combining the two effects, we write

$$B_{ex} = B_{ex}^{30\,nm}\frac{30\,nm}{t_{FM}}\exp\left(\frac{-t_{Cu}}{\lambda}\right), \quad (8)$$

where $B_{ex}^{30\,nm}$ is the exchange bias field for $t_{FM} = 30$ nm and $t_{Cu} = 0$ nm, and λ is the decay length.

B. Sensor self-heating

In the DC limit, the power P dissipated in the sensor is

$$P = R_b I_x^2 = V_x^2/R_b. \quad (9)$$

At steady-state, the entire Joule heating is dissipated to the surroundings

$$P = G_{eff}\Delta T, \quad (10)$$

where G_{eff} is the effective heat conductance and ΔT is the temperature difference between the sensor and the surroundings. For the same experimental setup and with a similar sensor structure, we have previously found a heat conductance of $G_{eff} = 0.02$ W/°C.[29]

C. Sensor response to beads magnetized by sensor self-field

The sensors can be used to detect magnetic beads. The current in the sensor generates a small magnetic field that magnetizes the beads in the proximity of the sensor surface. The magnetized beads generate a dipole magnetic field that allows their detection with no need for other external magnetic fields. The magnetic field from the beads (B_b) is proportional to the sensor bias current[7,15,18,19] and can be written as

$$B_b = \gamma I_x = \gamma\frac{V_x}{R_b}, \quad (11)$$

where γ is a proportionality factor depending on the bead properties and their distribution (compared to our previous work,[7,15] to keep the notation simple, we here include a factor of μ_0 in γ and the current is the total sensor current I_x). Combining Eqs. (6) and (11), the sensor output signal from magnetic beads can be written as

$$V_y = \gamma\tilde{S}_0 R_b I_x^2 = \gamma\tilde{S}_0 V_x^2/R_b = \gamma\tilde{S}_0 P. \quad (12)$$

Here, we have explicitly written the results in the DC limit when the sensor is current-driven, voltage-driven, and power-driven, respectively.

III. EXPERIMENTAL

A. Sensor fabrication

The four magnetoresistive sensor elements of each sensor bridge had a length $l = 250\,\mu$m and width $w = 20\,\mu$m (Fig. 1(a)). The sensor stack Ta(13 nm)/$Ni_{80}Fe_{20}$(t_{FM})/Cu(t_{Cu})/$Mn_{80}Ir_{20}$(10 nm)/Ta(3 nm) was deposited on a Si/SiO_2(1000 nm) substrate (Fig. 1(b)) in a Lesker CMS-18 magnetron sputter system. The easy direction was defined along the x-direction via deposition in a magnetic field of 20 mT. The sensor structure was surrounded by the same magnetic stack with a gap of 3 μm to reduce effects of shape anisotropy.[27] Sensor stacks with all combinations of $t_{FM} = 10$, 20, or 30 nm and $t_{Cu} = 0$, 0.3, or 0.6 nm were fabricated and characterized. For $t_{FM} = 10$ nm, the study further included $t_{Cu} = 0.15$, 0.45, and 0.75 nm. Thus, a total of twelve stack combinations were studied. Electrical contacts of Ti(5 nm)/Pt(100 nm)/Au(100 nm)/Ti(5 nm) were deposited by electron beam evaporation and defined by lift-off. A 1000 nm thick protective coating of Ormocomp (micro resist technology GmbH, Berlin, Germany) was spin-coated and defined by UV lithography.

B. Experimental characterization

The magnetic behavior of the stacks was characterized by easy axis hysteresis loop measurements on chips with a $3 \times 3\,mm^2$ lithographically defined square in a LakeShore model 7407 VSM.

Values of the ratio $\Delta\rho/\rho_{avg}$ were calculated from 4-point resistance measurements on a transmission line structure aligned along the x-direction in a magnetic field of 40 mT applied along and perpendicular to the structure. The sensor bridge resistances were obtained by 2-point resistance measurements. Both types of measurements were performed using a Keithley 2000 digital multimeter.

The electrical response of the sensors was characterized with the sensors mounted in a microfluidic system at a temperature of 25.0 ± 0.1 °C as described elsewhere.[7] The cross-section of the microfluidic channel over the sensor was 1 mm × 1 mm.

The response of the PHEB sensors to a homogeneous external field B_y swept in both directions between ±11 mT was characterized using a setup with a homebuilt Helmholtz coil. During the measurements, the sensor was biased by an alternating current with an amplitude of 1 mA provided by a Keithley 6221 precision current source at a frequency of 167 Hz. The sensor output was measured using a Stanford Research Systems (SRS) SR830 lock-in amplifier after 100× pre-amplification by an SR552 voltage pre-amplifier. All results were corrected for the pre-amplification. The sensor response to the external magnetic field was recorded in the 1st harmonic in-phase signal, V_1'.[15] The results were analyzed in terms of the single magnetic domain model, Eqs. (2) and (3), for the sensor signal vs. field. Parameters in the fits were $R_b\Delta\rho/\rho_{avg}$, B_{ex}, B_K, and B_{sh}.

The response of the PHEB sensors to a magnetic bead suspension magnetized by the sensor self-field was measured using the same setup. In these measurements, a sensor bias current of amplitude 20 mA was supplied at a frequency of 167 Hz. This frequency was chosen to obtain a measurement time of about 1 s per point with low noise. Furthermore, it is well below the Brownian relaxation frequency of the magnetic particles, such that magnetic response is essentially in-phase with the magnetic field (phase shift of 10° or less).[17] The in-phase magnetic response to the magnetic beads was

measured in the 2nd harmonic out-of-phase sensor response, V_2'' as described previously.[15–18] This signal has the same form as the simpler DC description presented in Eq. (12). The response to a homogeneous suspension of plain 80 nm BNF-Starch beads from Micromod (Rostock, Germany) diluted in Milli-Q water to a concentration of 10 mg/ml was measured as follows: First, the sensor baseline signal was measured with Milli-Q water in the fluidic channel for 1 min. Then, the bead suspension was injected in the microfluidic channel, and the sensor response was measured over a period of 5 min to reach a stable sensor signal. The bead signal, $\Delta V_2''$, was calculated as the corresponding signal variation.

IV. RESULTS

A. VSM measurements

The values of B_{ex} and B_K were extracted from easy axis hysteresis loops measured for all twelve stack compositions. The filled points in Fig. 2 show B_{ex} vs. t_{Cu} for the indicated values of t_{FM}. The dashed lines are a fit of Eq. (8) to the measurements with $\lambda = 0.43(2)$ nm and $B_{ex}^{30\,nm} = 2.1(1)$ mT. The experimental values are observed to be well described by the model. The obtained value of λ agrees well with that of $\lambda = 0.41$ nm reported by Gökemeijer *et al.*[21] Supplementary Figure S1 presents an example of a measured hysteresis loop as well as a plot of B_K corresponding to that in Fig. 2.[22]

B. Single domain model analysis of sensor field sweeps

Field sweeps of the sensor response measured at a fixed amplitude of the alternating bias current were analyzed in terms of the described single domain model. Free parameters in the fits were R_b $\Delta\rho/\rho_{avg}$, B_{ex}, and B_{sh}. A fit with B_K as a free parameter resulted in B_K being constant within the uncertainty, and therefore, this parameter was fixed to its average value of $B_K = 0.72$ mT in the further analysis. The single domain model was found to provide a good representation of all measured field sweeps (Supplementary Figure S2).[22] The value of the sensitivity $\tilde{S}_0 R_b$ was obtained from the slope of the fitted curve at $B_y = 0$. All results are plotted vs. t_{Cu} for the indicated values of t_{FM}.

Figure 2 shows the values of B_{ex} obtained from the single domain model fits of the sensor field sweeps (open symbols) as well as those obtained by VSM measurements (filled symbols). The values obtained by the two independent methods are found to be in excellent agreement for all values of t_{FM} and t_{Cu}.

Figure 3(a) shows the measured values of the sensor bridge resistance R_b obtained by 2-point measurements. As expected, R_b increases for decreasing t_{FM}. For a fixed value of t_{FM} and most pronounced for $t_{FM} = 10$ nm, R_b is found to decrease slightly when t_{Cu} is increased.

Figure 3(b) shows the values of $\Delta\rho/\rho_{avg}$ obtained from measurements on the transmission line test structure (filled symbols) and from single domain fits of the sensor field sweeps (open symbols). The latter values were calculated by dividing the values of $R_b\Delta\rho/\rho_{avg}$ obtained from the fits by the measured values of R_b. The values from the two measurements are in good agreement. For $t_{FM} = 20$ nm and 30 nm, the values are approximately independent of the stack composition and in the range 1.5%–1.7%. For $t_{FM} = 10$ nm, the

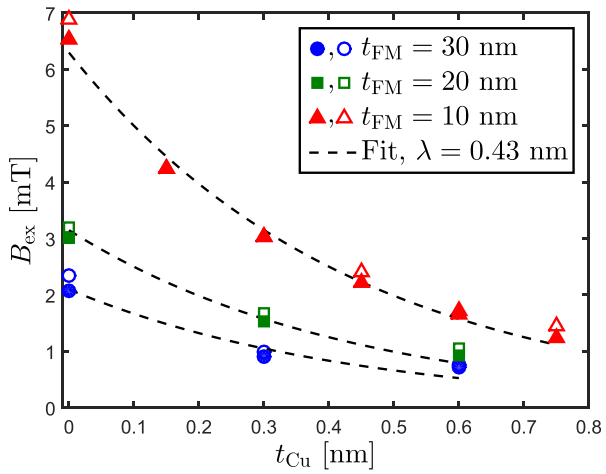

FIG. 2. Exchange bias field, B_{ex}, obtained from easy axis hysteresis loops measured by VSM (filled symbols) and from single domain model analysis of the sensor field sweeps (open symbols). The values are plotted for the indicated values of t_{Cu} and t_{FM}. The dashed lines are a fit of Eq. (8) to the VSM data with $\lambda = 0.43(2)$ nm and $B_{ex}^{30\,nm} = 2.1(1)$ mT.

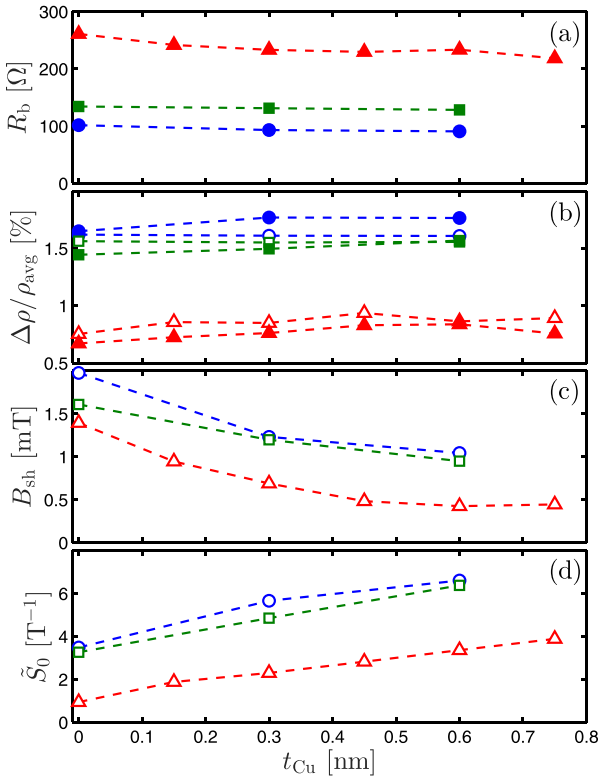

FIG. 3. Values vs. t_{Cu} for the indicated values of t_{FM} of (a) the bridge resistance R_b, (b) the AMR ratio $\Delta\rho/\rho_{avg}$, (c) the equivalent single domain shape anisotropy field B_{sh}, and (d) the normalized low-field sensitivity $\tilde{S}_0$. Circles, squares, and triangles correspond to $t_{FM} = 30$, 20, and 10 nm, respectively. Values with open symbols were obtained from fits to field sweeps of the sensor response, and values with filled symbols were obtained from electrical measurements on the sensor bridge (panel a) or on a transmission line structure (panel b). The lines are guides to the eye.

values of $\Delta\rho/\rho_{avg}$ are significantly lower and in the range 0.7%–0.8%.

Figure 3(c) shows the values of the shape anisotropy field B_{sh} obtained from the single domain fits of the sensor field sweeps. For fixed t_{Cu}, B_{sh} is observed to increase for increasing values of t_{FM}. For fixed t_{FM}, B_{sh} is found to decrease with increasing t_{Cu}. This decrease is larger for $t_{FM} = 30$ nm than for $t_{FM} = 20$ nm, such that the values of B_{sh} are approximately the same for these two values of t_{FM} when $t_{Cu} \geq 0.3$ nm.

Figure 3(d) shows the values of the normalized low-field sensitivity $\tilde{S}_0$. $\tilde{S}_0$ is found to increase with increasing t_{Cu}. The values obtained for $t_{FM} = 20$ nm and 30 nm are nearly identical and with a maximum value of $6.6\,T^{-1}$. For $t_{FM} = 10$ nm, the values are about 50% of those obtained for the stacks with $t_{FM} > 10$ nm.

C. Response to magnetic beads magnetized by sensor self-field

The sensor response to a homogeneous bead solution was measured as the variation, $\Delta V_2''$, in the second harmonic out-of-phase signal upon injection of the magnetic bead suspension. An example of experimental data and the extraction of $\Delta V_2''$ are given in supplementary Figure S3.[22] Figure 4 shows the values of $\Delta V_2''$ obtained for all twelve sensor stacks.

Figure 4(a) shows the magnetic bead signal, $\Delta V_2''$, measured for stacks with the indicated values of t_{Cu} and t_{FM}, when the sensors are biased by an alternating current of amplitude $I_x = 20$ mA. For $t_{Cu} = 0$, the sensors with $t_{FM} = 20$ nm show the highest signal. For increasing t_{Cu}, the signal for the sensor with $t_{FM} = 10$ nm is initially lower, but increases faster than for the other values of t_{FM} such that the signals for $t_{FM} = 10$ nm and 20 nm are identical for $t_{Cu} = 0.6$ nm. It should be noted that the sensor self-heating is higher for the sensor with the thinner permalloy layer. Using the measured value of R_b in Eq. (9) and $G_{eff} = 0.02$ W/°C, we estimate a sensor self-heating of about 2.5 °C for $t_{FM} = 10$ nm and 0.6 °C for $t_{FM} = 20$ nm, respectively. Thus, for this current, the self-heating of sensors with $t_{FM} = 10$ nm is significant.

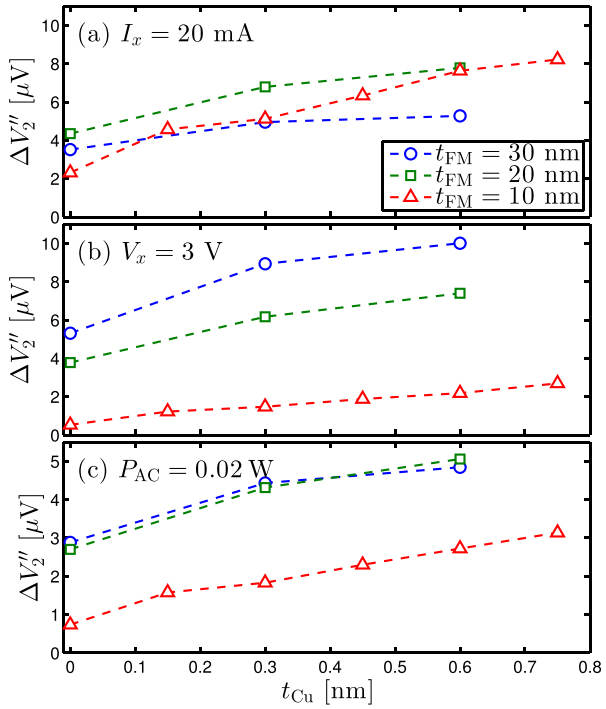

FIG. 4. (a) Measured sensor response to a magnetic bead suspension, $\Delta V_2''$, obtained vs. t_{Cu} for the indicated values of t_{FM} with sensors biased by an alternating current of amplitude $I_x = 20$ mA. (b) Sensor response measured for constant current rescaled to represent responses for sensors driven by an AC voltage of amplitude $V_x = 3$ V. (c) Sensor response measured for constant current rescaled to represent responses for sensors driven by an average AC power of $P_{AC} = 0.02$ W, corresponding to a sensor self-heating of $\Delta T = 1$ °C. The lines are guides to the eye.

It is also interesting to compare the signals when the sensors are biased using an AC voltage of fixed amplitude. This type of sensor operation is relevant when the sensor bias voltage must be maintained below a certain limit imposed by, for example, the integrity of the sensor and its coating when exposed to a buffer in the microfluidic channel. Figure 4(b) shows the results of Fig. 4(a) rescaled to represent values measured for an AC voltage of fixed amplitude $V_x = 3$ V. In this case, the magnetic bead signal in the DC limit, Eq. (12), is $V_y = \gamma\tilde{S}_0 V_x^2/R_b$, and thus, its magnitude is determined by the value of $\tilde{S}_0/R_b$. The maximum signal is clearly observed for $t_{FM} = 30$ nm with $t_{Cu} = 0.6$ nm, and sensors with larger values of t_{FM} and t_{Cu} generally show a higher signal. The main reason for this is the reduction of R_b for increasing t_{FM} combined with the reduction of B_{ex} for increasing values of t_{Cu} and t_{FM}.

Finally, assuming that the magnitude of the sensor bias current is limited by the sensor self-heating, the measured magnetic bead signals can be rescaled to be presented for a fixed allowable self-heating. In this case, the magnetic bead signal in the DC limit, Eq. (12), is $V_y = \gamma\tilde{S}_0 P$, and thus, its magnitude is determined by the value of $\tilde{S}_0$ that depends only on the properties of the sensor stack. Figure 4(c) shows the data from Fig. 4(a), rescaled to represent an average AC power consumption of $P_{AC} = 0.02$ W, corresponding to a sensor self-heating of $\Delta T = 1$ °C (Sec. II B). In this case, the sensors with $t_{FM} = 20$ nm and $t_{FM} = 30$ nm show a similar signal for each value of t_{Cu} investigated. The signals for the sensors with these two permalloy thicknesses are always higher than those for the sensors with $t_{FM} = 10$ nm. As expected, the variation of the $\Delta V_2''$ values for constant power closely mirrors that of $\tilde{S}_0$ in Fig. 3(d).

In general, for all the fabricated sensors stacks and the detection methods in Fig. 4, the bead signal was seen to increase for increasing values of t_{Cu}. Moreover, except for current-biased detection, higher signals are generally observed for $t_{FM} > 10$ nm.

V. DISCUSSION

A. Effects of t_{Cu} and t_{FM} on sensor behavior

The sensor sensitivity and the magnetic bead signal are directly influenced by $\Delta\rho/\rho_{avg}$, B_{ex}, B_K, and B_{sh}, and indirectly influenced by R_b. The former parameters affect the normalized low-field sensitivity $\tilde{S}_0$, and the latter parameter limits the maximum bias current that can be applied due to self-heating.

The value of $\Delta\rho/\rho_{avg}$ was found to be essentially independent of t_{FM} and t_{Cu} for the investigated sensor stacks when $t_{FM} > 10\,nm$. For $t_{FM} = 10\,nm$, the AMR ratio was found to be reduced by about 40%. These results are well in line with the literature.[30,31]

Thus, for $t_{FM} > 10\,nm$ and negligible shape anisotropy, the normalized low-field sensitivity $\tilde{S}_0$, Eq. (7), is determined by $B_{ex} + B_K$. The values of B_{ex} obtained from VSM measurements and analysis of the sensor field sweeps were in excellent agreement, and were found to be well described by Eq. (8). As B_K depended only little on the stack composition, one would expect to observe the highest value of $\tilde{S}_0$ for the stack with the largest values of t_{FM} and t_{Cu}. However, our results showed only a marginal increase in $\tilde{S}_0$ upon an increase of t_{FM} from 20 nm to 30 nm. This is caused by the increased influence of shape anisotropy for larger values of t_{FM} (see Fig. 3(c) for $t_{Cu} = 0\,nm$), which reduces the low-field sensitivity.[27] For fixed t_{FM}, the values of B_{sh} were observed to decrease with increasing t_{Cu}. We attribute this observation to a relaxation of the magnetic state near the sensor edges away from the single domain state, such that the magnetic pole density at the sensor edge is reduced.[27] The edge magnetic relaxation may co-exist with a vertical spring-like domain wall in the thickness direction of the permalloy layer.[32] However, in our previous studies, no significant indications of such a relaxation were observed for permalloy thicknesses up to 50 nm.[33] The edge relaxation becomes more energetically favorable when the exchange-pinning is weakened, and therefore, the effective single domain shape anisotropy B_{sh} is reduced. The combined effect of the shape anisotropy and reduction of B_{ex} for the investigated sensor geometry and stack compositions was that no gain in $\tilde{S}_0$ could be obtained by increasing t_{FM} above 20 nm (Fig. 3(d)).

The effective shape anisotropy field should fulfill $B_{sh} < B_{ex} + B_K$ to ensure a hysteresis-free sensor response.[27] For $t_{FM} = 20\,nm$ and $t_{Cu} = 0.6\,nm$, we found that $B_{sh} \approx 1\,mT$ and $B_{ex} + B_K \approx 1.6\,mT$. Hence, we expect that t_{Cu} can only be increased little beyond 0.6 nm before the sensor response becomes hysteretic, i.e., the value of $t_{Cu} = 0.6\,nm$ is close to optimal.

The value of the bridge resistance, R_b, was found to decrease with increasing t_{FM} in a non-trivial manner, while we found it to be largely independent of t_{Cu} for the investigated values. This dependence is determined by the current shunting through the non-permalloy layers as well as the dependence of the permalloy resistivity on t_{FM}.

If the sensor is used to measure external magnetic fields at a fixed, low amplitude of the bias current, the largest output is obtained for the sensor with the highest value of $R_b\tilde{S}_0$, see Eq. (6). Combining our measured values of R_b and $\tilde{S}_0$, we found the highest value $R_b\tilde{S}_0 = 1020\,\Omega/\,T$ for the stack with $t_{FM} = 10\,nm$ and $t_{Cu} = 0.75\,nm$.

Hung *et al.*[23] studied cross-shaped PHE sensors with magnetic stacks Ta(3)/NiFe(10)/Cu(t_{Cu})/MnIr(10)/Ta(3) (thicknesses in nm). When they introduced a copper layer with thickness $t_{Cu} = 0.2\,nm$, they found a sensitivity increase from $R_b\tilde{S}_0 = 16\,\Omega/T$ to 120 Ω/T compared to $t_{Cu} = 0\,nm$. The sensitivity increase was due to the exchange field decreasing from 12.5 mT to 1.5 mT. For our PHEB sensors with $t_{FM} = 10\,nm$, we observed an increase of the field sensitivity from $R_b\tilde{S}_0 = 295\,\Omega/T$ to 545 Ω/T due to B_{ex} decreasing from 6.5 mT to 4.2 mT when t_{Cu} increased from 0 nm to 0.15 nm. Comparing the results, we find that the exchange field measured by Hung *et al.* was higher without a copper layer and decreased more when the copper was introduced, which resulted in a higher relative increase of the field sensitivity. We attribute these differences in the exchange field to differences in the fabrication process and resulting thin film quality. Further, the total field sensitivity was higher for the PHEB sensors compared to the cross-shape PHE sensors due to the higher R_b of the bridge sensors.

B. Consequences for magnetic bead detection

The ideal sensor has a linear and hysteresis-free response for all experienced fields. To fulfil the linearity requirement, the sensed magnetic field should be small compared to $B_{ex} + B_K$. In the experiments in Fig. 4(a), we measured a bead signal corresponding to a magnetic bead field of $B_b = \gamma I_x \approx 0.4\,\mu T$, which is three orders of magnitude lower than typical values of $B_{ex} + B_K$. Hence, the sensors clearly operate in the low-field regime for magnetic bead detection.

In Fig. 4, we compared the magnetic bead signals when sensors with the different stack compositions were driven by current, voltage, or power of fixed magnitude.

For the current-driven case, Fig. 4(a), the sensor with $t_{FM} = 10\,nm$ and $t_{Cu} = 0.75\,nm$ was found to provide the largest signal as this stack composition yielded the largest sensitivity to a constant magnetic field, and the magnetic bead signal was constant. By comparing the bead signal to the baseline signal noise, taken as the measured standard deviation of the baseline signal in the bead detection experiments, we can estimate the limit of detection of the system in terms of bead field B_b (supplementary Figure S4).[22] The baseline noise was found to be largely independent of the stack composition, and we attribute it to be due to noise in the detection electronics. For the sensor with the highest bead signal at fixed amplitude of the bias current ($t_{FM} = 10\,nm$, $t_{Cu} = 0.75\,nm$), we estimated a limit of detection (taken as the field where the signal equals three times the standard deviation of the baseline signal) of $B_b = 0.5$ nT corresponding to a bead concentration of 13 μg/ml. As the sensor is mainly sensitive to magnetic beads close to the sensor, we can use the results of Hansen *et al.*[19] to estimate that most of the signal is due to beads in a volume over the four sensor branches of $V \approx 2l\pi(1.3w)^2 = 1.1$ nl. Combining this with the mass density of the magnetic beads of 3200 kg/m^3 specified by the manufacturer, we estimate that the signal from a bead concentration of 13 μg/ml is generated by approximately 1.6×10^4 beads in suspension. However, as previously noted, this sensor stack is subject to significant self-heating at a current of 20 mA.

For the voltage-driven case, Fig. 4(b), the sensor with $t_{FM} = 30\,nm$ and $t_{Cu} = 0.6\,nm$ was found to provide the largest signal, because this stack exhibited the highest value of $\tilde{S}_0/R_b$. The use of voltage-limited sensor bias may be used, for example, if the sensor is damaged when the voltage

exceeds a certain value due to failure of the sensor coating. If the sensor geometry can be designed freely, a voltage limit can be mitigated by reducing the sensor length l to make the sensor operation limited by the sensor self-heating.

For the power-driven case, Fig. 4(c), the sensors with $t_{FM} = 20\,nm$ and $30\,nm$ with $t_{Cu} = 0.6\,nm$ provided the largest signal. At fixed power, the signal for these stacks was found to be about 65% larger than that the stack with $t_{FM} = 10\,nm$ and $t_{Cu} = 0.75\,nm$, which was best stack identified for the current-driven case. Moreover, the signal was about 90% higher than that obtained for the stack with $t_{FM} = 20\,nm$ and $t_{Cu} = 0\,nm$ used in our previous studies.[7,14] Operation of a given sensor geometry at fixed power ensures that the maximum signal is obtained with a controlled influence of the sensor self-heating. As mentioned above, the sensor length can be tailored to additionally respect constraints on the applied voltage with minimal influence on $\tilde{S}_0$ as long as the sensor length l is much larger than the sensor width w. A change of w will affect both B_{sh} and γ in a non-trivial manner.

For detection of magnetic beads using the sensor self-field, we have justified that the normalized low-field sensitivity, $\tilde{S}_0$, as a good figure of merit for the performance of a stack. Our experimental investigation has shown that the optimal stack for detection of magnetic beads using the sensor self-field can be different from that for detection of magnetic fields, as the sensor signal for the former case scales with the power of the sensor bias current, whereas in the latter case, it scales with the sensor bias voltage.

VI. CONCLUSION

We have experimentally tested twelve different magnetic stacks for bead detection using the sensor self-field. All were characterized magnetically and for their application to magnetic bead detection. As expected, we found that a copper spacer layer exponentially decreased the exchange field, which in turn increased the signal from external magnetic fields and magnetic beads. When the magnetic bead signal was rescaled to a fixed power consumption corresponding to sensor self-heating limited operation, we found that the stacks with $t_{FM} = 20\,nm$ or $30\,nm$ and $t_{Cu} = 0.6\,nm$ were optimal and provided a 90% higher signal that the corresponding sensors with $t_{Cu} = 0$. For magnetic field detection using a constant current amplitude, the stack with $t_{FM} = 10$ and $t_{Cu} = 0.75\,nm$ provided the highest signal. The results show that the optimum stack depends on the sensor operation conditions. The introduced normalized low-field sensitivity provides a good figure of merit to compare sensor stacks for magnetic bead detection using the sensor self-field at constant power operation.

ACKNOWLEDGMENTS

G.R. acknowledges support from the Danish Council for Independent Research (Postdoc project, DFF-4005-00116).

[1]J. Llandro, J. J. Palfreyman, A. Ionescu, and C. H. W. Barnes, "Magnetic biosensor technologies for medical applications: A review," Med. Biol. Eng. Comput. **48**, 977–998 (2010).
[2]D. Issadore, Y. I. Park, H. Shao, C. Min, K. Lee, M. Liong, R. Weissleder, and H. Lee, "Magnetic sensing technology for molecular analyses," Lab Chip **14**, 2385–2397 (2014).
[3]Y. R. Chemla, H. L. Grossman, Y. Poon, R. McDermott, R. Stevens, M. D. Alper, and J. Clarke, "Ultrasensitive magnetic biosensor for homogeneous immunoassay," Proc. Natl. Acad. Sci. **97**, 14268–14272 (2000).
[4]S. X. Wang and G. L. G. Li, "Advances in giant magnetoresistance biosensors with magnetic nanoparticle tags: Review and outlook," IEEE Trans. Magn. **44**, 1687–1702 (2008).
[5]R. S. Gaster, D. A. Hall, C. H. Nielsen, S. J. Osterfeld, H. Yu, K. E. Mach, R. J. Wilson, B. Murmann, J. C. Liao, S. S. Gambhir, and S. X. Wang, "Matrix-insensitive protein assays push the limits of biosensors in medicine," Nat. Med. **15**, 1327–1332 (2009).
[6]D. A. Hall, R. S. Gaster, T. Lin, S. J. Osterfeld, S. Han, B. Murmann, and S. X. Wang, "GMR biosensor arrays: A system perspective," Biosens. Bioelectron. **25**, 2051–2057 (2010).
[7]G. Rizzi, F. W. Østerberg, M. Dufva, and M. Fougt Hansen, "Magnetoresistive sensor for real-time single nucleotide polymorphism genotyping," Biosens. Bioelectron. **52**, 445–451 (2014).
[8]Y. Wang, W. Wang, L. Yu, L. Tu, Y. Feng, T. Klein, and J. Wang, "Giant magnetoresistive-based biosensing probe station system for multiplex protein assays," Biosens. Bioelectron. **70**, 61–68 (2015).
[9]F. Nguyen Van Dau, A. Schuhl, J. Childress, and M. Sussiau, "Magnetic sensors for nanotesla detection using planar Hall effect," Sens. Actuators, A **53**, 256–260 (1996).
[10]L. Ejsing, M. F. Hansen, A. K. Menon, H. A. Ferreira, D. L. Graham, and P. P. Freitas, "Planar Hall effect sensor for magnetic micro- and nanobead detection," Appl. Phys. Lett. **84**, 4729 (2004).
[11]A. Schuhl, F. N. Van Dau, and J. R. Childress, "Low-field magnetic sensors based on the planar Hall effect," Appl. Phys. Lett. **66**, 2751 (1995).
[12]J. S. Moodera, L. R. Kinder, T. M. Wong, and R. Meservey, "Large magnetoresistance at room temperature in ferromagnetic thin film tunnel junctions," Phys. Rev. Lett. **74**, 3273 (1995).
[13]S. G. Grancharov, H. Zeng, S. Sun, S. X. Wang, S. O'Brien, C. B. Murray, J. R. Kirtley, and G. A. Held, "Bio-functionalization of monodisperse magnetic nanoparticles and their use as biomolecular labels in a magnetic tunnel junction based sensor," J. Phys. Chem. B **109**, 13030–13035 (2005).
[14]F. W. Østerberg, G. Rizzi, M. Donolato, R. S. Bejhed, A. Mezger, M. Strömberg, M. Nilsson, M. Strømme, P. Svedlindh, and M. F. Hansen, "On-chip detection of rolling circle amplified DNA molecules from Bacillus globigii spores and Vibrio cholerae," Small **10**, 1–23 (2014).
[15]F. W. Østerberg, G. Rizzi, T. Zardán Gómez de la Torre, M. Strömberg, M. Strømme, P. Svedlindh, and M. F. Hansen, "Measurements of Brownian relaxation of magnetic nanobeads using planar Hall effect bridge sensors," Biosens. Bioelectron. **40**, 147–152 (2013).
[16]F. W. Østerberg, G. Rizzi, A. D. Henriksen, and M. F. Hansen, "Planar Hall effect bridge geometries optimized for magnetic bead detection," J. Appl. Phys. **115**, 184505 (2014).
[17]F. W. Østerberg, G. Rizzi, and M. F. Hansen, "On-chip measurements of Brownian relaxation of magnetic beads with diameters from 10 nm to 250 nm," J. Appl. Phys. **113**, 154507 (2013).
[18]F. W. Østerberg, B. T. Dalslet, D. Snakenborg, C. Johansson, and M. F. Hansen, "Chip-based measurements of brownian relaxation of magnetic beads using a planar hall effect magnetic field sensor," AIP Conf. Proc. **1311**, 176–183 (2010).
[19]T. B. G. Hansen, C. D. Damsgaard, B. T. Dalslet, and M. F. Hansen, "Theoretical study of in-plane response of magnetic field sensor to magnetic beads magnetized by the sensor self-field," J. Appl. Phys. **107**, 124511 (2010).
[20]A. D. Henriksen, S. X. Wang, and M. F. Hansen, "On the importance of sensor height variation for detection of magnetic labels by magnetoresistive sensors," Sci. Rep. **5**, 12282 (2015).
[21]N. Gökemeijer, T. Ambrose, and C. Chien, "Long-range exchange bias across a spacer layer," Phys. Rev. Lett. **79**, 4270–4273 (1997).
[22]See supplementary material at http://dx.doi.org/10.1063/1.4943033. Figure S1 shows and example of an easy axis hysteresis loop and a plot of B_K vs. t_{Cu} obtained from VSM measurements for all stack compositions. Figure S2 shows the measured field sweeps for sensors with $t_{FM} = 10$, 20, and 30 nm and $t_{Cu} = 0$, 0.3, and 0.6 nm as well as fits of the single domain model to the data. Figure S3 shows examples of magnetic bead detection experiments. Figure S4 shows measured signal-to-noise ratios in bead detection experiments and corresponding estimates of the limit of detection.

[23]T. Q. Hung, S. Oh, S. Anandakumar, J. R. Jeong, D. Y. Kim, and C. Kim, "Optimization of the multilayer structures for a high field-sensitivity biochip sensor based on the planar Hall effect," IEEE Trans. Magn. **45**, 4518–4521 (2009).
[24]T. Q. Hung, S. Oh, B. Sinha, J.-R. Jeong, D.-Y. Kim, and C. Kim, "High field-sensitivity planar Hall sensor based on NiFe/Cu/IrMn trilayer structure," J. Appl. Phys. **107**, 09E715 (2010).
[25]B. Sinha, T. Q. Hung, T. S. Ramulu, S. Oh, K. Kim, D.-Y. Kim, F. Terki, and C. Kim, "Planar Hall resistance ring sensor based on NiFe/Cu/IrMn trilayer structure," J. Appl. Phys. **113**, 063903 (2013).
[26]A. D. Henriksen, B. T. Dalslet, D. H. Skieller, K. H. Lee, F. Okkels, and M. F. Hansen, "Planar Hall effect bridge magnetic field sensors," Appl. Phys. Lett. **97**, 013507 (2010).
[27]A. D. Henriksen, G. Rizzi, and M. F. Hansen, "Experimental comparison of ring and diamond shaped planar Hall effect bridge magnetic field sensors," J. Appl. Phys. **118**, 103901 (2015).
[28]J. Nogués and I. K. Schuller, "Exchange bias," J. Magn. Magn. Mater. **192**, 203–232 (1999).
[29]A. D. Henriksen, G. Rizzi, F. W. Østerberg, and M. F. Hansen, "Optimization of magnetoresistive sensor current for on-chip magnetic bead detection using the sensor self-field," J. Magn. Magn. Mater. **380**, 209–214 (2015).
[30]V. Gehanno, P. P. Freitas, A. Veloso, J. Ferreira, B. Almeida, J. B. Sousa, A. Kling, J. C. Soares, and M. F. da Silva, "Ion beam deposition of Mn-Ir spin valves," IEEE Trans. Magn. **35**, 4361–4367 (1999).
[31]N. T. Thanh, L. T. Tu, N. D. Ha, C. O. Kim, C. Kim, K. H. Shin, and B. Parvatheeswara Rao, "Thickness dependence of parallel and perpendicular anisotropic resistivity in Ta/NiFe/IrMn/Ta multilayer studied by anisotropic magnetoresistance and planar Hall effect," J. Appl. Phys. **101**, 053702 (2007).
[32]R. Morales, Z.-P. Li, O. Petracic, X. Batlle, and I. K. Schuller, "Magnetization depth dependence in exchange biased thin films," Appl. Phys. Lett. **89**, 072504 (2006).
[33]C. D. Damsgaard, S. C. Freitas, P. P. Freitas, and M. F. Hansen, "Exchange-biased planar Hall effect sensor optimized for biosensor applications," J. Appl. Phys. **103**, 07A302 (2008).